Available online at www.sciencedirect.com

ScienceDirect

Mendeleev Commun., 2020, **30**, 563–566

Mendeleev Communications

Synthesis, characterization and redox properties of Ar–C=N→Ge←N=C–Ar containing system

Irina V. Krylova,[a] Evgeniya A. Saverina,[a,b] Stanislav S. Rynin,[a] Andrey V. Lalov,[a] Mikhail E. Minyaev,[a] Elena N. Nikolaevskaya,[a] Mikhail A. Syroeshkin[a] and Mikhail P. Egorov*[a]

[a] *N. D. Zelinsky Institute of Organic Chemistry, Russian Academy of Sciences, 119991 Moscow, Russian Federation. E-mail: en@ioc.ac.ru, mpe@ioc.ac.ru*

[b] *Institut des Sciences Chimiques de Rennes, University of Rennes, UMR CNRS 6226, Rennes, France*

DOI: 10.1016/j.mencom.2020.09.003

New Schiff base germanate derivative containing the chain Ar–C=N→Ge←N=C–Ar was synthesized and characterized by physical methods including X-ray diffraction. The stability of the corresponding radical anion obtained electrochemically was confirmed by cyclic voltammetry, the results were compared with UV-VIS data and quantum chemical calculations.

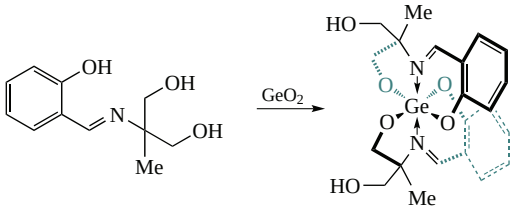

Keywords: germanium complexes, salens, redox chemistry, Schiff bases, cyclic voltammetry, radical ions, DFT calculations.

Organometallic and coordination compounds containing redox-active ligands retain a constant and stable interest[1] since one of the most widespread and affordable way to influence properties of any compound is electron transfer.[2] Implementation of organic compartments capable of electron transfer into the sphere of metal allows one to supply a product with a variety of magneto-chemical[3] and optoelectronic properties,[4] the target biological activity,[5] to develop prospective photovoltaic materials,[6] energy storage devices,[7] medicine,[8] catalysis[9] as well as new generation of molecular machines.[10]

Organic derivatives of the main group elements is of particular interest due to the urgency of searching for new catalytic systems that do not contain transition metals.[11] Germanium derivatives are the promising compounds,[12] for example, in infrared optics,[13] medicine[14] and high-capacity lithium-ion batteries.[15] Meanwhile, studies on electrochemical properties of germanium derivatives with redox-active ligands are episodic.[16]

In this paper we present the first germanium derivative giving a highly stable (in time scale of physical methods) radical anion being in the meantime easily oxidizable. This compound was obtained from 2-iminophenol **1** and GeO_2 in water (Scheme 1), so that the germanium atom in product **2** became located in the center of the redox-active chain Ar–C=N→Ge←N=C–Ar closed by donor–acceptor bonds but is rigidly fixed by the surrounding covalent ones. High resolution mass spectrum of complex **2** performed with H^+, Na^+ and K^+ ionization procedure shows a group of peaks corresponding to the germanium species with its characteristic polyisotopic pattern (for details, see Online Supplementary Materials).

Single crystals of **2** were obtained by cooling of a saturated MeOH solution.† The molecular structure of **2** is depicted in Figure 1. The Ge–O and Ge–N distances in **2** are comparable to those in similar compounds **3**–**7**. The Ge(1)–O(1) bond length [1.8563(14) Å] is slightly shorter than those in **3** (1.87 Å),[21] **4** (1.871 Å),[22] **5** (2.017 Å),[23] **6** (1.938 Å),[23] and **7** (1.924 and 1.928 Å).[23] The Ge(1)–O(3) bond length [1.8759(14) Å] is

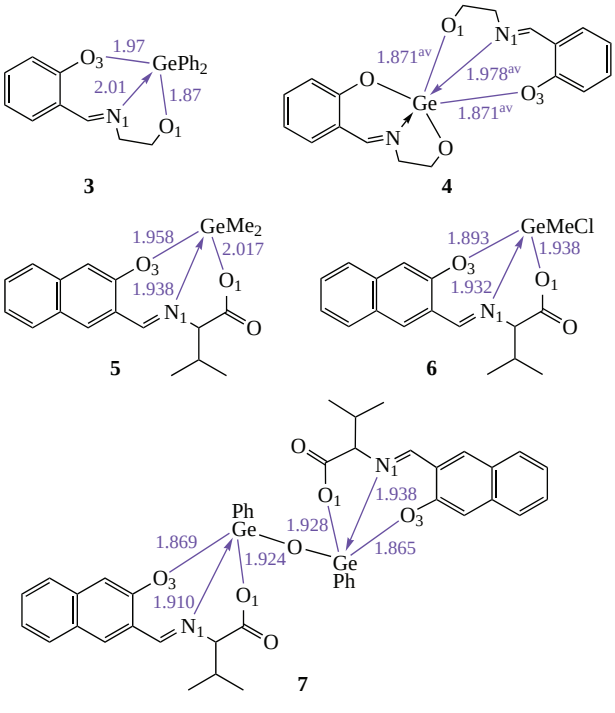

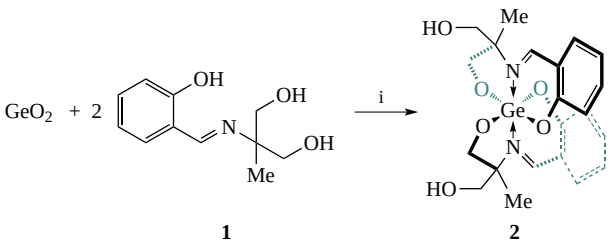

Scheme 1 *Reagents and conditions*: i, H_2O, reflux, 5 h.

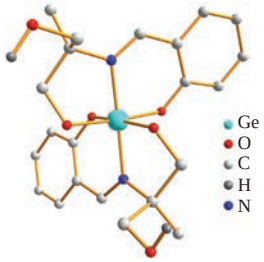

Figure 1 Molecular structure of **2**. Hydrogen atoms except H at hydroxyl groups are omitted for clarity.

slightly shorter than those in **3** (1.97 Å), **4** (1.871 Å), **5** (1.958 Å), **6** (1.893 Å), and **7** (1.869 and 1.865 Å). Value of Ge(1)–N(1) bond in **2** [1.9850(15) Å] lies in the range typical for donor–acceptor bond lengths of aforementioned atoms.[24] Atoms N(1), Ge(1) and N(1A) make almost straight line – angle N(1)–Ge(1)–N(1A) is 174.12°.

Redox properties of compound **2** have been investigated by cyclic voltammetry in DMF and MeCN (Figure 2 and Table 1). Compound **2** would be easily oxidized [see Figure 2(*a*)], which is confirmed by the presence of irreversible peak at potentials 1.39 V (in MeCN) or 1.48 V (in DMF). At the same time, the oxidation of **2** is more difficult thermodynamically in contrast to free ligand **1** (1.08 V in MeCN and 1.16 V in DMF, respectively), whose electrochemical behavior is typical of phenols. These differences in redox potentials satisfy the stabilization of redox active motif on 7 kcal mol^{-1} after complexing with germanium. In all cases the oxidation leads to irreversible formation of unstable radical cation according to the ECE mechanism (electron transfer–proton elimination–electron transfer).

The reduction of **2** takes place in more affordable potential region in contrast to the reduction of **1** [see Figure 2(*b*),(*c*)] that corresponds also with stabilization of redox center by donation of electron pair to germanium and LUMO level decreasing. Furthermore, electron transfer to ligand **1** occurs irreversibly, and the species undergoes some further chemical reaction [see Figure 2(*b*)]. In contrast, electroreduction of **2** is accompanied by the formation of very stable radical anion. This complies with the existence of one electron reversible peak on the CV curve including at the different rates of potential overlap (the dependence of the forward and reverse peak currents on the square root of the potential scan rate is linear) and, also,

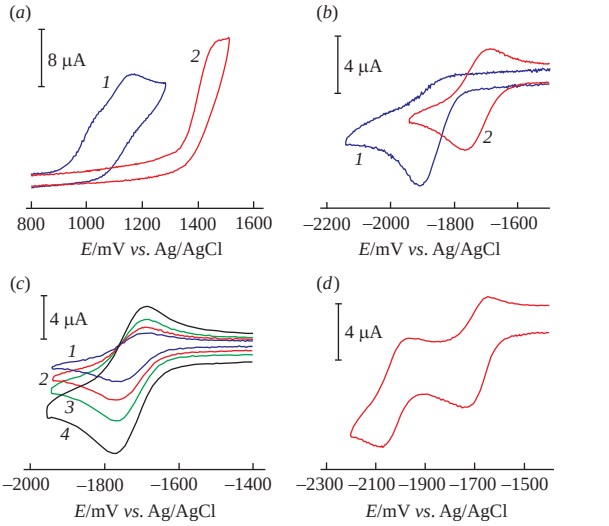

Figure 2 CV curves: (*a*) oxidation of (*1*) 1 mmol dm^{-3} **1** in comparison with (*2*) oxidation of 2 mmol dm^{-3} **2** in DMF at potential scan rate of 0.1 V s^{-1}; (*b*) reduction of (*1*) 1 mmol dm^{-3} **1** in comparison with (*2*) reduction of 2 mmol dm^{-3} **2** in DMF at potential scan rate of 0.1 V s^{-1}; (*c*) reduction of 1 mmol dm^{-3} **2** in DMF at potential scan rates of (*1*) 0.05, (*2*) 0.1, (*3*) 0.2 and (*4*) 0.4 V s^{-1}; (*d*) two-stage reduction of 1 mmol dm^{-3} **2** in MeCN at potential scan rate of 0.1 V s^{-1}. In all cases electrolyte is 0.1 M Bu_4NBF_4, working electrode is glassy carbon (GC) disc (d = 1.7 mm), T = 298 K.

proximity to the theoretical value 59 mV of the potential difference between the cathode and anode peaks when approximating to zero current.

Further, it was found out that transfer of the first as well as the second electrons is reversible and is not accompanied by followed chemical reactions. Thus, it gives stable dianion that complies with existence of reversible peak at far potential region scanning [see Figure 2(*d*)]. On this basis, we can conclude that the second electrophoric ligand participates in the redistribution of the extra electron.

Ligand **1** is brightly yellow in solid state as well as in the solution, while germanium derivative **2** is pale yellow. This manifests typically on UV-VIS spectra (Figure 3) where **1** absorbs in visible region (up to 450 nm), deleting blue part of spectra, whereas the absorption of **2** is close to violet region (at 410 nm and less). Maxima at 405 and 368 nm in MeCN or 408 and 369 nm in DMF, respectively, correspond to electron transition between the near energy levels in compounds **1** and **2** after photoexcitation. This complies with energy of ~3.05 and 3.36 eV and correlates with difference of oxidation/reduction potentials of aforementioned compounds (see Table 1).

The optimized at DFT level of theory geometry of **2** and its corresponding radical cation and radical anion is not particularly different from starting geometry, given from X-ray experiment (for details, see Online Supplementary Materials). The character of the population of HOMO and LUMO of **2** shows their distribution over the organic ligand part of the complex, which correlates with the electrochemically obtained data indicating a key role in the oxidation and reduction of **2** redox active fragments (see Table 1). The calculated energy difference between the HOMO and LUMO is 4.23 eV, which indicates the high stability of the molecule. According to these data, the electron transfer in compound **2** is accompanied by the following change in the distribution of the electron density of the HOMO and geometry in the radical cation and radical anion.

Based on the results of calculating the distribution of the electron density of the HOMO corresponding to compound **2** as well as its corresponding radical cation and radical anion, we can conclude that changes in the electron density in the course of

† *Crystal data for* **2**. $C_{22}H_{26}GeN_2O_6$ (M = 487.04), monoclinic, space group $C2/c$ at 100(2) K, a = 19.763(3), b = 12.6113(19) and c = 8.4960(12) Å, β = 92.510(3)°, V = 2115.4(5) Å^3, Z = 4, d_{calc} = 1.529 g cm^{-3}, μ(MoKα) = 1.491 mm^{-1}, F(000) = 1008. Total of 29407 reflections were collected [3218 independent reflections with $I > 2\sigma(I)$, R_{int} = 0.0631] and used in the refinement, which converged to wR_2 0.0842, GOOF 1.086 for all independent reflections [R_1 = 0.0363 was calculated for 3218 reflections with $I > 2\sigma(I)$].

X-ray diffraction data were collected on a Bruker Quest D8 diffractometer equipped with a Photon-III area-detector (graphite monochromator, shutterless φ- and ω-scan technique), using MoKα-radiation (0.71073 Å). The intensity data were integrated by the SAINT program[17] and were corrected for absorption and decay using SADABS.[18] The structure was solved by direct methods using SHELXS[19] and refined on $F2$ using SHELXL-2018.[20] All non-hydrogen atoms were refined with individual anisotropic displacement parameters. The location of atom H(2) was found from the electron density-difference map; it was refined with an individual isotropic displacement parameter. All other hydrogen atoms were placed in ideal calculated positions and refined as riding atoms with relative isotropic displacement parameters. The SHELXTL program suite[17] was used for molecular graphics.

CCDC 2002880 contains the supplementary crystallographic data for this paper. These data can be obtained free of charge from The Cambridge Crystallographic Data Centre *via* http://www.ccdc.cam.ac.uk.

Table 1 Peak potential of oxidation (E^{p}_{ox}), reduction (E^{p}_{red1} and E^{p}_{red2}), and half-wave potentials ($E^{1/2}_{red1}$ and $E^{1/2}_{red2}$) on glassy carbon disc electrode *vs.* Ag/AgCl (0.1 M Bu_4NBF_4). Absorption maxima of **1** and **2** in DMF and MeCN (and corresponding energy value of HOMO/LUMO electron transition) and difference of LUMO and HOMO energy of **2** in gas phase (quantum chemical calculations).

Solvent		E^{p}_{ox}/V	E^{p}_{red1}/V	$E^{1/2}_{red1}$/V	E^{p}_{red2}/V	$E^{1/2}_{red2}$/V	E^{p}_{ox}–E^{p}_{red1}/V	λ/nm (eV)	E^{LUMO}–E^{HOMO}/eV
MeCN	**1**	1.080	–1.819	–	–	–	2.90	405 (3.06)	–
	2	1.388	–1.704	–1.672	–2.050	–2.011	3.09	368 (3.37)	4.23
DMF	**1**	1.165	–1.905	–	–	–	3.07	408 (3.04)	–
	2	1.479	–1.757	–1.723	–2.170	–2.128	3.24	369 (3.36)	4.23

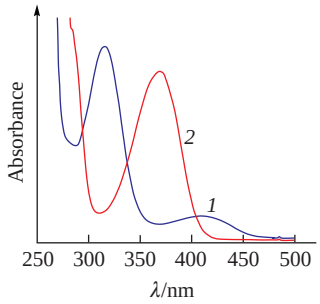

Figure 3 UV-VIS spectra of (*1*) ligand **1** (2×10^{-4} M) and (*2*) complex **2** (1×10^{-4} M) in DMF.

oxidation and reduction of compound **2** occur exclusively in the ligand environment of germanium, without significant changes in geometric parameters. This allows us to conclude that the use of Schiff base ligands is an effective way to obtain redox active complexes of germanium in which the central atom is rigidly fixed by the framework of covalent Ge–O and Ge–N bonds, and the central motif Ar–C=N→Ge←N=C–Ar forms a system capable of sending and receiving electrons, including reversibly.

This work was supported by the Russian Science Foundation (grant no. 18-73-10180). Crystal structure determination was performed in the Department of Structural Studies of N. D. Zelinsky Institute of Organic Chemistry, Moscow.

Online Supplementary Materials

Supplementary data associated with this article can be found in the online version at doi: 10.1016/j.mencom.2020.09.003.

References

1 (*a*) G. A. Abakumov, A. V. Piskunov, V. K. Cherkasov, I. L. Fedushkin, V. P. Ananikov, D. B. Eremin, E. G. Gordeev, I. P. Beletskaya, A. D. Averin, M. N. Bochkarev, A. A. Trifonov, U. M. Dzhemilev, V. A. D'yakonov, M. P. Egorov, A. N. Vereshchagin, M. A. Syroeshkin, V. V. Jouikov, A. M. Muzafarov, A. A. Anisimov, A. V. Arzumanyan, Yu. N. Kononevich, M. N. Temnikov, O. G. Sinyashin, Yu. H. Budnikova, A. R. Burilov, A. A. Karasik, V. F. Mironov, P. A. Storozhenko, G. I. Shcherbakova, B. A. Trofimov, S. V. Amosova, N. K. Gusarova, V. A. Potapov, V. B. Shur, V. V. Burlakov, V. S. Bogdanov and M. V. Andreev, *Russ. Chem. Rev.*, 2018, **87**, 393; (*b*) E. N. Nikolaevskaya, N. O. Druzhkov, M. A. Syroeshkin and M. P. Egorov, *Coord. Chem. Rev.*, 2020, **417**, 213353.

2 M. A. Syroeshkin, F. Kuriakose, E. A. Saverina, V. A. Timofeeva, M. P. Egorov and I. V. Alabugin, *Angew. Chem., Int. Ed.*, 2019, **58**, 5532.

3 (*a*) O. Sato, *Nat. Chem.*, 2016, **8**, 644; (*b*) V. Ovcharenko, O. Kuznetsova, E. Fursova, G. Letyagin, G. Romanenko, A. Bogomyakov and E. Zueva, *Inorg. Chem.*, 2017, **56**, 14567; (*c*) S. A. Nikolaevskii, M. A. Kiskin, A. G. Starikov, N. N. Efimov, A. S. Bogomyakov, V. V. Minin, E. A. Ugolkova, O. M. Nikitin, T. V. Magdesieva, A. A. Sidorov and I. L. Eremenko, *Russ. J. Coord. Chem.*, 2019, **45**, 273 (*Zh. Koord. Khim.*, 2019, **45**, 219).

4 C. O'Brien, M. Y. Wong, D. B. Cordes, A. M. Z. Slawin and E. Zysman-Colman, *Organometallics*, 2015, **34**, 13.

5 U. el-Ayaan and A. A.-M. Abdel-Aziz, *Eur. J. Med. Chem.*, 2005, **40**, 1214.

6 J. W. Kee, Y. Y. Ng, S. A. Kulkarni, S. K. Muduli, K. Xu, R. Ganguly, Y. Lu, H. Hirao and H. S. Soo, *Inorg. Chem. Front.*, 2016, **3**, 651.

7 J. Winsberg, T. Hagemann, T. Janoschka, M. D. Hager and U. S. Schubert, *Angew. Chem.. Int. Ed.*, 2017, **56**, 686.

8 P. Mounkoro, T. Michel, S. Blandin, M.-P. Golinelli-Cohen, E. Davioud-Charvet and B. Meunier, *Free Radical Biol. Med.*, 2019, **141**, 269.

9 (*a*) S. Sandl, T. M. Maier, N. P. van Leest, S. Kröncke, U. Chakraborty, S. Demeshko, K. Koszinowski, B. de Bruin, F. Meyer, M. Bodensteiner, C. Herrmann, R. Wolf and A. J. von Wangelin, *ACS Catal.*, 2019, **9**, 7596; (*b*) I. S. Fomenko, A. L. Gushchin, L. S. Shul'pina, N. S. Ikonnikov, P. A. Abramov, N. F. Romashev, A. S. Poryvaev, A. M. Sheveleva, A. S. Bogomyakov, N. Y. Shmelev, M. V. Fedin, G. B. Shul'pin and M. N. Sokolov, *New J. Chem.*, 2018, **42**, 16200; (*c*) A. S. Hazari, R. Ray, M. A. Hoque and G. K. Lahiri, *Inorg. Chem.*, 2016, **55**, 8160.

10 V. Romanovs, J. Spura and V. Jouikov, *Synthesis*, 2018, **50**, 3679.

11 (*a*) T. Chu and G. I. Nikonov, *Chem. Rev.*, 2018, **118**, 3608; (*b*) C. Weetman and S. Inoue, *ChemCatChem*, 2018, **10**, 4213; (*c*) A. M. Yakub, M. V. Moskalev, N. L. Bazyakina and I. L. Fedushkin, *Russ. Chem. Bull., Int. Ed.*, 2018, **67**, 473 (*Izv. Akad. Nauk, Ser. Khim.*, 2018, 473); (*d*) T. A. Egiazaryan, V. M. Makarov, M. V. Moskalev, D. A. Razborov and I. L. Fedushkin, *Mendeleev Commun.*, 2019, **29**, 648; (*e*) A. M. Yakub, M. V. Moskalev, N. L. Bazyakina, A. V. Cherkasov, A. S. Shavyrin and I. L. Fedushkin, *Russ. Chem. Bull., Int. Ed.*, 2016, **65**, 2887 (*Izv. Akad. Nauk, Ser. Khim.*, 2016, 2887); (*f*) S. S. Karlov, G. S. Zaitseva and M. P. Egorov, *Russ. Chem. Bull., Int. Ed.*, 2019, **68**, 1129 (*Izv. Akad. Nauk, Ser. Khim.*, 2019, 1129).

12 (*a*) R. Dasgupta, S. Das, S. Hiwase, S. K. Pati and S. Khan, *Organometallics*, 2019, **38**, 1429; (*b*) T. Y. Lai, K. L. Gullett, C.-Y. Chen, J. C. Fettinger and P. P. Power, *Organometallics*, 2019, **38**, 1421; (*c*) Y. Wu, C. Shan, Y. Sun, P. Chen, J. Ying, J. Zhu, L. Liu and Y. Zhao, *Chem. Commun.*, 2016, **52**, 13799; (*d*) T. J. Hadlington, M. Hermann, G. Frenking and C. Jones, *J. Am. Chem. Soc.*, 2014, **136**, 3028; (*e*) R. R. Aysin, S. S. Bukalov, L. A. Leites, A. V. Lalov, K. V. Tsys and A. V. Piskunov, *Organometallics*, 2019, **38**, 3174; (*f*) R. K. Siwatch and S. Nagendran, *Chem. – Eur. J.*, 2014, **20**, 13551.

13 (*a*) J. Shi, F. Han, C. Cui, Y. Yu and X. Feng, *Opt. Commun.*, 2020, **459**, 125093; (*b*) I. Yonenaga, in *Single Crystals of Electronic Materials. Growth and Properties*, ed. R. Fornari, Woodhead Publishing, 2019, pp. 89–127; (*c*) Z. Cui, Z. Pan, W. Ren, C. Jin and X. Yu, *Proc. SPIE 11185, Optical Design and Testing IX*, 2019, 1118511; (*d*) J. Kang, Z. Cheng, W. Zhou, T.-H. Xiao, K.-L. Gopalakrisna, M. Takenaka, H. K. Tsang and K. Goda, *Opt. Lett.*, 2017, **42**, 2094; (*e*) J. Tian, H. Luo, Q. Li, X. Pei, K. Du and M. Qiu, *Laser Photonics Rev.*, 2018, 1800076.

14 (*a*) G. E. Filonova, E. N. Nikolaevskaya, A. V. Kansuzyan, I. V. Krylova, M. P. Egorov, V. V. Jouikov and M. A. Syroeshkin, *Eur. J. Org. Chem.*, 2019, 4128; (*b*) E. N. Nikolaevskaya, A. V. Kansuzyan, G. E. Filonova, V. A. Zelenova, V. M. Pechennikov, I. V. Krylova, M. P. Egorov, V. V. Jouikov and M. A. Syroeshkin, *Eur. J. Inorg. Chem.*, 2019, 676; (*c*) A. A. Vishtorskaya, E. A. Saverina, V. M. Pechennikov, I. V. Krylova, A. V. Lalov, M. A. Syroeshkin, M. P. Egorov and V. V. Jouikov, *J. Organomet. Chem.*, 2018, **858**, 8; (*d*) H. Matsumoto, H. Iwafuji, J. Yamane, R. Takeuchi, T. Utsunomiya and A. Fujii, *Wound Med.*, 2016, **15**, 6; (*e*) L. Li, T. Ruan, Y. Lyu and B. Wu, 2017, **5**, 56; (*f*) K. Marino, R. Lee and P. Lee, *Orthop. J. Sports Med.*, 2019, doi. org/10.1177/2325967119879124; (*g*) J. Hu, Q. Lu, C. Wu, M. Liu, H. Li, Y. Zhang and S. Yao, *Langmuir*, 2018, **34**, 8932.

15 (*a*) Y. Wang, S. Luo, M. Chen and L. Wu, *Adv. Funct. Mater.*, 2020, **30**, 2000373; (*b*) E. A. Saverina, V. Sivasankaran, R. R. Kapaev, A. S. Galushko, V. P. Ananikov, M. P. Egorov, V. V. Jouikov, P. A. Troshin and M. A. Syroeshkin, *Green Chem.*, 2020, **22**, 359; (*c*) E. A. Saverina, R. R. Kapaev, P. V. Stishenko, A. S. Galushko, V. A. Balycheva, V. P. Ananikov, M. P. Egorov, V. V. Jouikov, P. A. Troshin and M. A. Syroeshkin, *ChemSusChem*, 2020, **13**, 3137.

16 (*a*) E. N. Nikolaevskaya, E. A. Saverina, A. A. Starikova, A. Farhati, M. A. Kiskin, M. A. Syroeshkin, M. P. Egorov and V. V. Jouikov, *Dalton Trans.*, 2018, **47**, 17127; (*b*) E. N. Nikolaevskaya, P. G. Shangin, A. A. Starikova, V. V. Jouikov, M. P. Egorov and M. A. Syroeshkin, *Inorg. Chim. Acta*, 2019, **495**, 119007.

17 *APEX3*, Bruker AXS., Madison, WI, USA, 2018.
18 L. Krause, R. Herbst-Irmer, G. M. Sheldrick and D. Stalke, *J. Appl. Crystallogr.*, 2015, **48**, 3.
19 G. M. Sheldrick, *Acta Crystallogr.*, 2015, **A71**, 3.
20 G. M. Sheldrick, *Acta Crystallogr.*, 2015, **C71**, 3.
21 L. E. H. Paul, I. C. Foehn, A. Schwarzer, E. Brendler and U. Böhme, *Inorg. Chim. Acta*, 2014, **423**, 268.
22 L. E. H. Paul, I. C. Foehn, A. Schwarzer, E. Brendler and U. Böhme, *Inorg. Chim. Acta*, 2015, **438**, 189.
23 S. Schwarzer, U. Böhme, S. Fels, B. Günther and E. Brendler, *Inorg. Chim. Acta*, 2018, **483**, 136.
24 S. S. Batsanov, *Russ. J. Inorg. Chem.*, 1991, **36**, 1694 (*Zh. Neorg. Khim.*, 1991, **36**, 3015).

Received: 11th May 2020; Com. 20/6216